Two murine cytomegalovirus microRNAs target the major viral immediate early 3 gene

Herb, Stefanie; Železnjak, Jelena; Hennig, Thomas; L'Hernault, Anne; Lodha, Manivel; Jürges, Christopher; Tršan, Tihana; Juranić Lisnić, Vanda; Jonjić, Stipan; Erhard, Florian; ...

Two murine cytomegalovirus microRNAs target the major viral immediate early 3 gene

Stefanie Herb[1]†, Jelena Zeleznjak[2]†, Thomas Hennig[1]†, Anne L'Hernault[3], Manivel Lodha[1], Christopher Jürges[1], Tihana Trsan[2], Vanda Juranic Lisnic[2], Stipan Jonjic[2], Florian Erhard[1], Astrid Krmpotic[2],* and Lars Dölken[1,3,4],*

Abstract

Human cytomegalovirus is responsible for morbidity and mortality in immune compromised patients and is the leading viral cause of congenital infection. Virus-encoded microRNAs (miRNAs) represent interesting targets for novel antiviral agents. While many cellular targets that augment productive infection have been identified in recent years, regulation of viral genes such as the major viral immediate early protein 72 (IE72) by hcmv-miR-UL112-1 may contribute to both the establishment and the maintenance of latent infection. We employed photoactivated ribonucleotide-enhanced individual nucleotide resolution crosslinking (PAR-iCLIP) to identify murine cytomegalovirus (MCMV) miRNA targets during lytic infection. While the PAR-iCLIP data were of insufficient quality to obtain a comprehensive list of cellular and viral miRNA targets, the most prominent PAR-iCLIP peak in the MCMV genome mapped to the 3′ untranslated region of the major viral immediate early 3 (*ie3*) transcript. We show that this results from two closely positioned binding sites for the abundant MCMV miRNAs miR-M23-2-3p and miR-m01-2-3p. Their pre-expression significantly impaired viral plaque formation. However, mutation of the respective binding sites did not alter viral fitness during acute or subacute infection *in vivo*. Furthermore, no differences in the induction of virus-specific CD8+ T cells were observed. Future studies will probably need to go beyond studying immunocompetent laboratory mice housed in pathogen-free conditions to reveal the functional relevance of viral miRNA-mediated regulation of key viral immediate early genes.

INTRODUCTION

Human cytomegalovirus (HCMV) is a major cause of morbidity in immunocompromised patients such as allogeneic bone marrow or organ transplant recipients [1]. Furthermore, it is the leading agent of birth defects among congenitally transmitted infections. During millions of years of coevolution with its human and animal hosts the virus has evolved to exploit a multitude of cellular mechanisms to support acute infection, establishment of latency and reactivation thereof. Virus-encoded microRNAs (miRNAs) represent a stealthy means for the virus to regulate both cellular and viral gene expression. To date, 22 mature HCMV miRNAs have been reported to originate from 12 pre-miRNA stem loops (reviewed in [2–5]). These are expressed either individually or in small clusters scattered throughout the viral genome. Extensive efforts by multiple groups have revealed numerous cellular and viral targets of the HCMV miRNAs (reviewed in [6–8]). These targets cover a broad spectrum of cellular pathways and mechanisms including apoptosis, cell cycle, intrinsic immunity, metabolism and signalling. As such, hcmv-miR-UL112-1 inhibits expression of the stress-induced natural killer (NK) cell activating ligand MICB thereby cooperating with viral proteins to protect the virus-infected cells against NK cell-mediated killing [9]. Interestingly, the same viral miRNA also targets the major

viral immediate early protein 72 (IE72) [10, 11]. The latter may augment the establishment of viral latency or suppress virus reactivation. Pre-expression of the respective viral miRNA, as may occur *in vivo* upon transmission from infected to uninfected cells via exosomes [12], inhibited productive virus replication in fibroblasts *in vitro*. Targeting this viral miRNA using antisense approaches may thus promote virus reactivation and disease. Interestingly, viral miRNA-mediated regulation of key immediate early transcripts appears to be a common feature independently developed by multiple different herpesviruses [10] including IE72 in HCMV [10, 11], RTA in Kaposi's sarcoma-associated herpesvirus (KSHV) [13], BZLF1 and BRLF1 in Epstein–Barr virus (EBV) [10, 14] as well as ICP0 and ICP4 in herpes simplex virus 1 (HSV-1) [15]. This is thought to suppress low amounts of viral immediate early gene expression spontaneously arising during the establishment and maintenance of latency, thereby protecting the latently infected cells from recognition and killing by IE-specific cytotoxic T cells [16].

We and others previously identified the murine cytomegalovirus (MCMV) to express 27 viral miRNAs from 18 pre-miRNA stem loops [17, 18]. Similar to HCMV, viral miRNAs are expressed either individually or in small clusters scattered throughout the viral genome. Although most of these miRNAs are expressed at very high levels during productive infection, large deletion mutants revealed the majority of them to be completely dispensable for productive infection *in vitro* [17]. In contrast, knockout of two viral miRNAs, namely miR-M23-2 and miR-m21-1, resulted in selective virus attenuation in salivary glands during subacute infection [19]. The underlying molecular mechanism remains to be determined.

Here, we report on the identification of two viral miRNAs binding sites in the major immediate early 3 (*ie3*) transcript, which encodes the major viral transcription factor. Pre-expression of the respective viral miRNAs significantly suppressed the initiation of lytic virus replication in murine fibroblasts. However, mutation of the respective binding sites had no detectable effect on viral fitness during both acute and subacute infection in mice. Finally, no effects on both conventional and inflationary CD8$^+$ T-cell responses could be observed.

METHODS

Cell lines and MCMV infection

TCMK-1 murine kidney epithelial cells (ATCC: CCL-139) and M2-10B4 bone marrow stroma cells (ATCC: CRL-1972) were cultured in Dulbecco's modified Eagle medium (DMEM) containing 10% FCS and penicillin/streptomycin. NIH-3T3 fibroblasts (ATCC: CRL-1658) were cultured in DMEM medium containing 5% FCS and penicillin/streptomycin.

Generation of mutant viruses

The dual colour reporter virus (MCMV-SCP-IRES-mCherry-m152-eGFP; m129-repaired) had previously been generated in our lab by *en passant* mutagenesis [20] using fully synthesized targeting constructs carrying a Zeocin resistance gene for the positive selection step (for details see Supplementary Methods). Mutant and revertant viruses for the *ie3* miRNA binding sites were generated both on the dual colour reporter virus background as well as on the wild-type MCMV BAC pSM3fr with repaired m129. All PCR primers are detailed in the Supplementary Methods. All mutant bacterial artificial chromosomes (BACs) were subjected to extensive restriction pattern analysis using at least three different restriction enzymes followed by sequencing of the altered *ie3* locus. Viruses were reconstituted by transfecting the recombinant BACs into murine NIH-3T3 fibroblasts. Viruses were grown on M2-10B4 cells and stocks produced as described [21]. A detailed description of the viruses employed in this study is included in the Supplementary Methods.

Multi-step growth kinetics assay

In vitro viral growth was analysed by infecting cultured primary BALB/c MEF with MCMV – WT, IE3 mutant (Clone 2-2) or revertant virus (Clone 2-2-1) at 0.1 p.f.u. per cell in a suspension, at a concentration of 10^7 cells ml^{-1} for 30 min with occasional agitation at 37 °C. Following incubation, the unbound virus was washed with media, and cells were pelleted three times for 5 min at 500 *g*. The cells were plated on a 48-well plate at a concentration of 0.2×10^6 cells per well. At indicated days post-infection (dpi), the triplicates of the cell-free culture supernatants were collected and stored at −80 °C. The amount of extracellular infectious virus present in the culture supernatant was determined by a standard plaque-forming assay.

MCMV infection for PAR-iCLIP

For the large-scale MCMV infections for photoactivated ribonucleotide-enhanced individual nucleotide resolution crosslinking (PAR-iCLIP), cells from seven 15 cm dishes (80% confluent) per condition (for MCMV infection) were trypsinized 3–4 days after the last split and resuspended in 1 ml cell culture medium per plate. MCMV stock was added at an m.o.i. of 5 (*t*=0). Similar to centrifugal enhancement, infecting cells in suspension rather than on plates improves infection efficacy by about 10-fold as the cells come into contact with many more virus particles in suspension. After 1 h of inoculation, cells were transferred to a bottle with 195 ml cell culture media containing a final concentration of 25 µM 4-thiouridine (4sU). Cells were plated on to ten 15 cm dishes (20 ml per plate). At 24 and 48 h post-infection (hpi), an additional 25 µM (24 hpi) and 50 µM (48 hpi) 4sU was added to the cell culture medium. Uninfected cells were split 24 h prior to the start of 4sU labelling (100 µM 24 h).

Small synthetic RNAs

MirVanda miRNA mimics for mcmv miR-m01-2-3p (MH13371) and mcmv-miR-M23-2-3p (MH13291), the small interfering RNA (siRNA) to *ie3* (#4399665; 5′-GTTCGACATGAGTTAAGATTGG-3′), a negative control miRNA (#4464058) for the dual luciferase reporter assays as well as the BLOCK-iT Fluorescent Oligo to control for small RNA transfection efficacies were all obtained from ThermoFisher.

Dual luciferase reporter assays

To validate miRNA binding sites in target 3′-untranslated regions (UTRs), we utilized the dual luciferase pSIcheck2 reporter [22] and cloned the MCMV *ie3* 3′-UTR (233 bp) downstream of firefly luciferase using recombinatorial (BP) cloning. For the perfect match positive controls, we generated the vector pSIcheck2-N1, which shows enhanced firefly luciferase signal due to the introduction of a more canonical TATA-box and altered 5′-UTR. Perfect match binding sites for either miR-m01-2-3p or miR-M23-2-3p were introduced by BP cloning. A detailed description of all employed reporter constructs is included in the Supplementary Methods. Co-transfection of reporter plasmids and miRNA mimics into HEK293T cells was performed using the TransIT-X3 Dynamic Delivery System (MIRUS Bio) following the manufacturer's instructions. HEK293T cells (4×10^4 cells in 100 µl of media per well, 96-well clear flat-bottom plates) were reverse transfected with 50 nM of miRNA mimic, 5 ng of pSIcheck2 reporter plasmids and 95 ng of an mCherry-expressing control plasmid (to monitor transfection efficiency) in technical triplicates per condition. Then, 24 h later, dual luciferase measurements were performed. Following removal of 40 µl of supernatant from all wells to reduce the culture medium volume to 50 µl per well, the Dual-Glow Luciferase Assay (Promega) was performed according to the manufacturer's instructions. In brief, 50 µl of Dual-Glo Reagent was added to each well. After 10 min of incubation at room temperature, firefly luciferase signals were measured on the Centro XS LB 960 Luminometer (Berthold Technologies). For measuring Renilla luminescence, Dual Glo Stop and Glo reagent was diluted 1:100 in Stop Glo Buffer. Then, 50 µl of this solution was added to each well, followed by 10 min of incubation at room temperature. Renilla luciferase signals were then measured as described for firefly luciferase.

For the MCMV infection experiments (Fig. 2d), 8×10^4 NIH-3T3 cells were seeded per well of a six-well dish. Twenty-four hours later, cells were infected with MCMV at an m.o.i. of 10. At 24 hpi cells were transfected using Lipofectamine with 450 ng pEGFP-N1 (plasmid expressing eGFP for transfection control) and 50 ng of the indicated pSIcheck2 reporter plasmids. At 72 hpi, dual luciferase activities were measured as described above. A detailed description of the plasmids employed in this study is included in the Supplementary Methods.

Western blot analysis

Immunoblot analyses for IE3 (polyclonal rabbit serum), IE1 (mouse anti-IE1: CROMA101) and β-tubulin (control) protein expression were performed as described [23]. Immunoblots were scanned at high resolution and band intensity was analysed using Fiji software.

Plaque suppression assay

NIH-3T3 cells were reverse transfected with 50 nM of both miR-m01-2 and miR-M23-2, the IE3 siRNA or the fluorescent small RNA control (see above) using the TransIT-X3 Dynamic Delivery System (MIRUS Bio) following the manufacturer's instructions. Transfection mixes were pipetted into the respective wells of an 48-well plate followed by the addition of 4.5×10^4 cells in 273 µl of complete medium per well. Then, 24 h later, cells were infected with either the dual colour miRNA binding site mutant reporter virus or its revertant aiming for ~100 plaques per well. Following 1 h of incubation at 37 °C, virus inoculum was replaced by 500 µl of carboxy-methylcellulose medium. Three days later, the total number of plaques as well as the number of small and large virus plaques were determined based on the mCherry (late gene) signal of the infected cells. We defined small plaques as containing up to three red cells and distinguished them from large plaques comprising more than three infected cells. To avoid examiner bias, plates were counted blinded to the employed condition.

Mice and infection

BALB/c and C57BL/6 mice were bred under specific pathogen-free conditions at the Faculty of Medicine, University of Rijeka. Eight- to 12-week-old females were infected with 2×10^4 or 10^5 p.f.u. per mouse of MCMV – WT, IE3 mutants (Clone 2-2 and Clone 4-2) or revertant virus (Clone 2-2-1). All viruses used for *in vivo* experiments were propagated on BALB/c mouse embryonic fibroblasts and titrated by standard plaque assay as described previously [24]. For determination of viral titres, BALB/c mice were infected with the indicated viruses, and titres in spleen, liver, salivary glands and lungs of individual mice were assessed at 4 dpi (intravenous infection, i.v.) and 14 dpi (intraperitoneal infection, i.p.) by standard plaque assay. For determination of memory CD8+ T-cell heterogeneity, mice were footpad inoculated with 10^5 p.f.u. per mouse of mutant (Clone 2-2) and revertant MCMV. Lymphocytes from spleen of infected BALB/c mice were isolated on the indicated days post-infection and stained with antibodies specific for selected surface markers.

Virus-specific CD8$^+$ T-cell stimulation

BALB/c or C57BL/6 mice were footpad infected with 10^5 pf.u. per mouse. After the indicated days post-infection, mice were killed and their spleen was isolated. Splenocytes from immunized mice were then incubated in the presence of $5 \mu g \, ml^{-1}$ MHC I-restricted and MCMV-specific custom synthesized peptides (JPT Peptide Technologies) together with Brefeldin A (1000×; Thermo Fisher Scientific) for 5h. For BALB/c mice, H-2^d-restricted m164 ($_{257}$AGPPRYSRI$_{265}$) and IE1 (pp89) ($_{168}$YPHFMPTNL$_{176}$) inflationary peptides were used. H-2^b-restricted inflationary M38 ($_{316}$SSPPMFRV$_{323}$), m139 ($_{419}$TVYGFCLL$_{426}$) and IE3 ($_{416}$RALEYKNL$_{423}$) and non-inflationary M45 ($_{985}$HGIRNASFI$_{993}$) peptides were added to C57BL/6 splenocytes. Production of IFNγ by CD8$^+$ T cells was assessed by flow cytometry.

Flow cytometry and intracellular cytokine staining

Single-cell suspensions of spleen were prepared according to standard protocols. Flow cytometric analyses were performed using the following anti-mouse antibodies: CD8$^+$ (clone 53-6.7), CD44 (clone IM7), KLRG1 (clone 2F1), CD127 (clone SB/199), CD62L (clone MEL-14) and IFNγ (clone XMG1.2), which were all purchased from Thermo Fisher Scientific, preceded by blocking of Fc receptors using 2.4G2 antibody (generated in house). Fixable viability dye eFluor780 (Thermo Fisher Scientific) was used for the discrimination between live and dead cells. The following peptides were obtained through JPT Peptide Technologies: H-2D^d MCMV m164 ($_{257}$AGPPRYSRI$_{265}$), H-2L^d MCMV IE1 (pp89) ($_{168}$YPHFMPTNL$_{176}$), H-2K^b MCMV M38 ($_{316}$SSPPMFRV$_{323}$), H-2K^b MCMV m139 ($_{419}$TVYGFCLL$_{426}$), H-2K^b MCMV IE3 ($_{416}$RALEYKNL$_{423}$) and H-2D^b MCMV M45 ($_{985}$HGIRNASFI$_{993}$). Tetramers specific for H-2D^d MCMV m164 ($_{257}$AGPPRYSRI$_{265}$) (m164-tetramer-PE) and H-2L^d MCMV IE1 (pp89) ($_{168}$YPHFMPTNL$_{176}$) (IE1-tetramer-BV421) were obtained from NIH Tetramer Core Facility. Intracellular staining, permeabilization and fixation of cells were done with the Fixation/Permeabilization kit (Thermo Fischer Scientific). Phorbol myristate acetate (PMA) (Sigma-Aldrich) and ionomycin (Sigma-Aldrich) were used to stimulate CD8$^+$ T cells as positive controls. Stimulation of CD8$^+$ T cells with viral-specific peptides was done in the presence of Brefeldin A (1000×; Thermo Fischer Scientific). All data were acquired using a FACSAriaIIu (BD Biosciences) and analysed using FlowJo v10 software (Tree Star). The gating strategy is described in detail in Fig. S5.

PAR-iCLIP

In total, 1×10^8 TCMK-1 murine epithelial cells were infected with wild-type MCMV at an m.o.i. of 5. One hour later, virus inoculum was replaced with fresh cell culture medium containing 25 μM 4sU. After 24 and 48 h of infection, +25 μM and +50 μM 4sU was added to the cell culture medium. Uninfected cells were labelled with 100 μM 4sU for 16 h. Prior to UV crosslinking at 365 nm on ice, cell culture medium was taken off the plates. Crosslinking was performed at 0.15 J cm^{-2} of 365 nm UV light using a Spectrolinker XL-1500 (Spectronics Corporation). Cells were harvested and iCLIP libraries were prepared using the monoclonal anti-mouse AGO2 antibody from Wako (Catalogue no. 018-2202) as described in detail [25]. The 3′ adapter sequence (AGATCGGAAGAGCGGTT) was trimmed using reaper [26], and library barcode sequences (first 9 nt of read=three random bases followed by four bases of sample-specific barcode followed by two random bases) were removed from all reads and stored for later use. All reads were mapped using bowtie 1.2 [27] against the murine genome and transcriptome (Ensembl version 90) and the MCMV genome and transcriptome (GenBank KY348373.1). To collapse random barcodes for each mapped read location, the most frequently observed sequence (composed of random barcode and mapped read sequence) was determined. This sequence and all sequences with exactly one mismatch (to account for sequencing errors) were removed. This procedure was repeated until no sequences remained. The number of iterations was used as the read count. This procedure was repeated separately for each sample-specific barcode. Barcodes not matching any sample-specific sequence were discarded. Mismatch frequencies and miRNA read counts were determined using GRAND-SLAM 2.0.7 [28].

Statistical analyses

Statistical significance was determined by a two-tailed unpaired Student's *t*-test, non-parametric Mann–Whitney U-test, two-way ANOVA or non-parametric one-way Kruskal–Wallis ANOVA using Graph Pad Prism software. Unless otherwise noted, data are presented as mean±SD. A value of $P>0.05$ was deemed not statistically significant (ns) and not shown on the graph; *$P<0.05$, **$P<0.01$ and***$P<0.001$.

RESULTS

PAR-iCLIP for MCMV miRNA target identification

To identify MCMV miRNA targets on a larger scale, we established PAR-iCLIP. This combines culturing MCMV-infected cells in the presence of the nucleoside analogue 4sU followed by 365 nm UV-crosslinking [29] and library preparation with the individual nucleotide resolution crosslinking protocol (iCLIP) [25]. To label cellular and viral transcripts expressed throughout lytic infection, we infected TCMK-1 murine epithelial cells at an m.o.i. of 5 and supplemented the cell culture media with 25 μM 4sU at both 0 and 24 hpi as well as 50 μM 4sU at 48 hpi (for experimental setup see Fig. 1a). Uninfected cells were labelled with 100 μM 4sU for 16 h
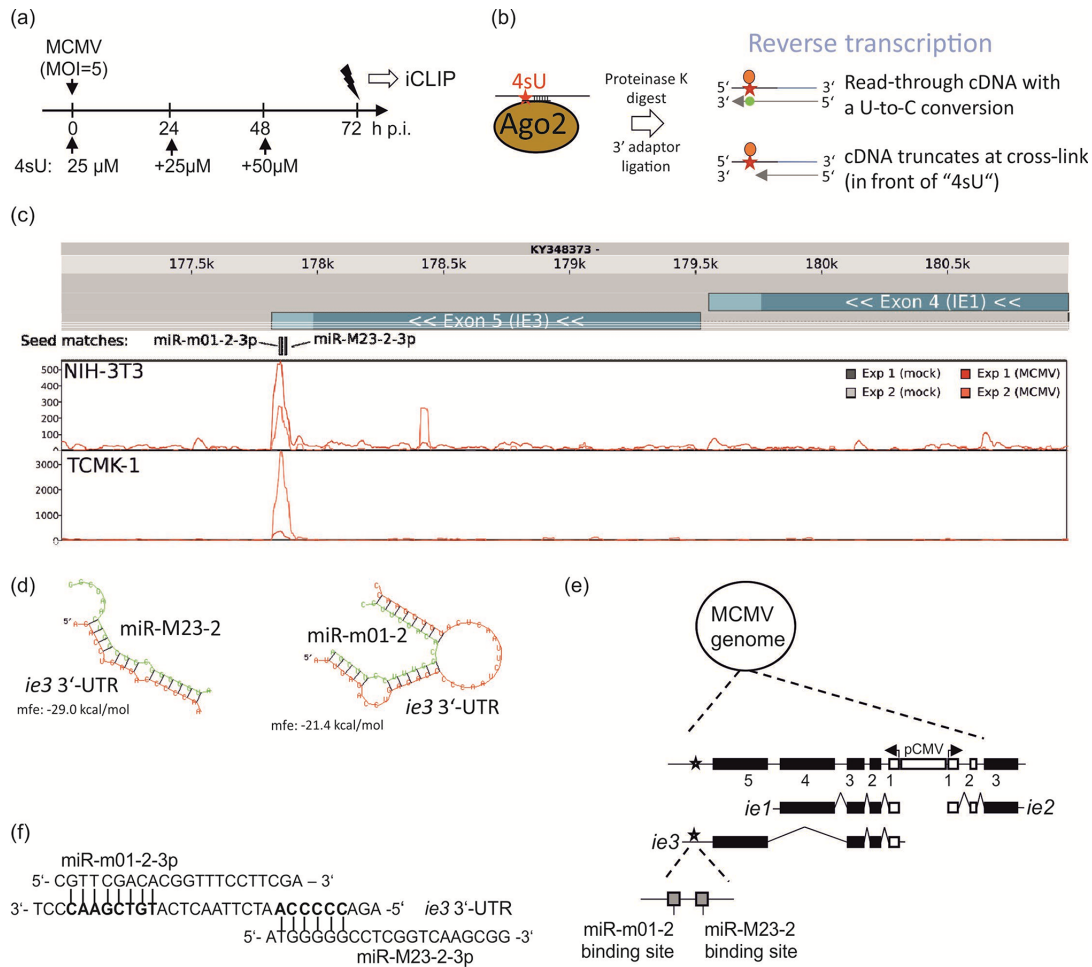
Fig. 1. PAR-iCLIP identifies two putative viral miRNA binding sites in the *ie3* 3′-UTR. (a) Schematic overview on the PAR-iCLIP cell culture conditions. In total, 1×10^8 TCMK-1 epithelial cells were infected with wild-type MCMV (m129 repaired) at an m.o.i. of 5. Metabolic RNA labelling was initiated by the addition of 4-thiouridine (4sU) to the cell culture medium at the indicated time points. Following UV crosslinking (365 nm) at 72 hpi cells were harvested and subjected to the iCLIP protocol as described [25]. (b) Schematic overview of PAR-iCLIP. Targets of cellular and viral miRNAs are cross-linked to Ago2 by 365 nm crosslinking at sites of 4sU incorporation. Following RNase digest and immunoprecipitation, a proteinase K digest removes most of the cross-linked Ago2 protein from the target RNA. Upon 3′ adaptor ligation, reverse transcription results in two different kinds of cDNAs. In case the reverse transcriptase manages to read through the 4sU crosslink, this results in a U-to-C conversion. However, many cDNAs truncate at the crosslink and thus end in front of a uridine residue (Fig. S1A). (c) PAR-iCLIP data of the MCMV *ie1/ie3* locus. Coverage of PAR-iCLIP reads within the MCMV immediate early gene locus (reverse strand) is shown for both NIH-3T3 (top) and TCMK-1 cells (bottom). The seed matches of the two MCMV miRNAs (mcmv-miR-M23-2 and -miR-m01-2) are indicated. The *ie3* 3′-UTR is indicated in light blue, exons in dark blue. (d) Putative binding sites for viral miR-M23-2-3p and miR-m01-2-3p in the *ie3* 3′-UTR as predicted by RNAhybrid [30]. Mean free energy (mfe) as a measure of the strength of interaction is indicated. (e) Genomic organization of the bidirectional MCMV major immediate-early region. The two transcription units *ie1/ie3* and *ie2* are both composed of several exons. Non-coding and coding exons are depicted as open and filled rectangles, respectively. Transcription in this region is controlled by the MCMV promoter and enhancer elements (pCMV). The three major spliced transcripts of MCMV are indicated. Due to a poly(A) signal shortly downstream of exon 4, the two miRNA binding sites are only present in the *ie3* transcript, which contains exon 5. (f) PAR-iCLIP identified two closely positioned binding sites for the MCMV-encoded miR-M23-2-3p and miR-m01-2-3p. Seed matches are indicated in bold.

prior to UV-crosslinking and cell lysis. Sequencing libraries were prepared using the iCLIP protocol [25]. In contrast to the commonly applied PAR-CLIP protocol [29], iCLIP is based on 3′ adapter ligation and circularization. In addition, it introduces five nucleotides of random barcode for *in silico* removal of PCR duplicates. Accordingly, the PAR-iCLIP sequencing reads either end one nucleotide before the UV-crosslink or extend through the site of 4sU crosslinking resulting in a U- to C-conversion (Fig. 1b, Fig. S1 and S2, available with the online version of this article). Evolutionarily conserved target sites of the top five cellular miRNAs expressed in murine fibroblasts and epithelial cells were significantly enriched in the obtained PAR-iCLIP data (Fig. S3). Unfortunately, hardly any prominent PAR-iCLIP read clusters were obtained within the cellular genome, indicating that the respective data still contained a problematic level of experimental noise. However, when looking for PAR-iCLIP clusters within the MCMV genome, we identified a
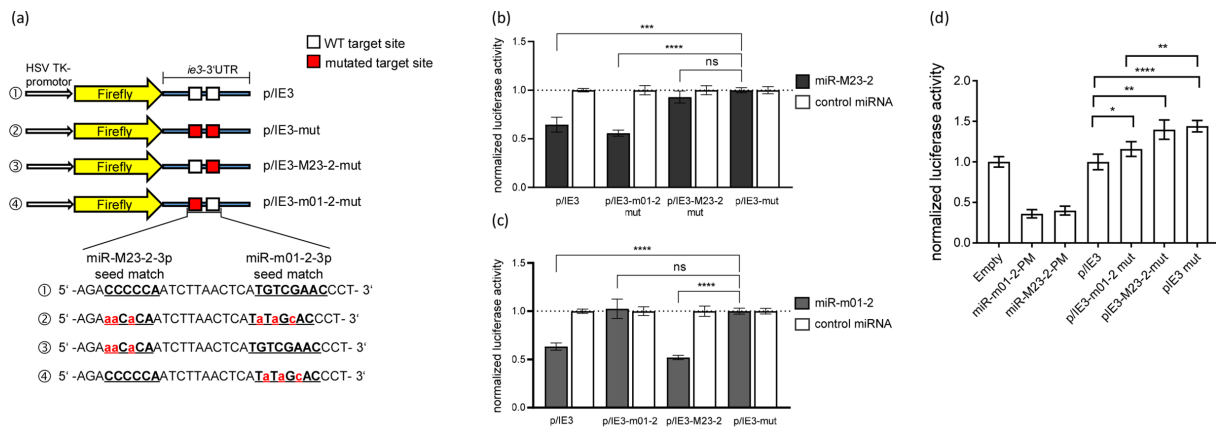
Fig. 2. MCMV regulates *ie3* expression by two of its virus-encoded miRNAs. (a) Dual luciferase reporter constructs generated for the validation of the *ie3* 3′-UTR target sites. Point mutations introduced to disrupt miRNA seed matches (underlined) are indicated in red. (b-c) HEK293T cells were co-transfected with the indicated dual luciferase reporters and miRNA mimics. Normalized firefly luciferase activities are shown. (d) NIH-3T3 cells were seeded into 24-well dishes and infected with wild-type MCMV at an m.o.i. of 10 the day thereafter. At 24 hpi, cells were transfected with 50 ng of indicated reporter plasmids together with 450 ng of the pEGFP-N1 plasmid per well. Dual luciferase measurements were performed at 72 hpi. Normalized firefly luciferase activities are shown. Note that miR-m01-2-PM and miR-M23-2-PM were normalized to the empty vector (empty), from which they were derived, while all three mutants of p/IE3 were normalized to p/IE3. Combined data (mean±SEM) of three (two for infection experiments in d) independent experiments are shown. *$P<0.05$; **$P<0.01$; ***$P<0.001$; ****$P<0.0001$.

strong PAR-iCLIP peak within the 3′ UTR of the viral immediate early 3 (*ie3*) transcript (Fig. 1c) in both MCMV-infected NIH-3T3 and TCMK-1 cells.

Two MCMV miRNAs target *ie3*

miRNA target predictions using RNAhybrid [30] indicated two viral miRNAs, namely mcmv-miR-M23-2 (miR-M23-2-3p: 6-mer seed match) and mcmv-miR-m01-2 (miR-m01-2-3p: 8-mer seed match) to bind 11 nt apart from each other within the identified *ie3* PAR-iCLIP cluster (Fig. 1d-f). Regulation by two rather than only a single MCMV miRNA was supported by the presence of U-to-C conversions both surrounding and in between the seed matches of the two viral miRNAs. In addition, PAR-iCLIP reads in MCMV-infected cells frequently ended at uridine residues both flanking and in between the seed matches of the two MCMV miRNAs (Fig. S4). To validate the respective predictions, we generated dual luciferase reporter constructs by cloning the full-length *ie3* 3′-UTR downstream of the firefly luciferase gene into the pSIcheck2-N1 dual-luciferase reporter plasmid (Fig. 2a). In addition, we mutated the putative seed matches for both viral miRNAs either individually or combined (Fig. 2a). Perfect match sensor constructs for both miR-M23-2 (miR-M23-2-PM) and miR-m01-2 (miR-m01-2-PM) served as positive controls. Co-transfection of the respective reporters with the two viral miRNAs confirmed both miRNAs binding sites within the *ie3* 3′-UTR with both sites mediating similar (≈50%) repression (Fig. 2b and c). To validate miRNA-mediated repression of the *ie3* in the context of MCMV infection, we infected NIH-3T3 murine fibroblasts at an m.o.i. of 10. At 24 hpi cells were transfected with the two perfect match reporter controls, the *ie3* 3′-UTR reporter or the respective single or double miRNA binding site mutants thereof. Dual luciferase activities were measured at 72 hpi (Fig. 2d). While both perfect match reporters showed an ≈60% repression, mutation of the miR-M23-2 binding site in the *ie3* 3′-UTR resulted in a significantly stronger release of repression than mutation of the miR-m01-2 binding site. Furthermore, derepression of the *ie3* 3′-UTR was significantly stronger for the double mutant than the miR-m01-2 binding site mutant. We conclude that miR-m01-2 and miR-M23-2 cooperate in the repression of the viral *ie3* gene with miR-M23-2 providing the stronger repression. Unfortunately, no antibody was available to confirm the regulation of IE3 at the protein level.

Pre-expression of the two viral miRNAs inhibits IE3 protein expression

To directly analyse the effect of the two miRNA binding sites in the *ie3* 3′-UTR, we generated a mutant virus (Clone 2-2) by disrupting the two respective miRNA seed sites on the wild-type MCMV background (m129 repaired) by the introduction of three point mutations (as shown in Fig. 2a) using BAC technology [20]. In addition, we generated the corresponding revertant virus (Clone 2-2-1) by restoring the wild-type sequence. Multi-step growth kinetic analysis on primary BALB/c murine embryonic fibroblasts demonstrated that both the mutant (Mut) and revertant virus (Rev) replicated with similar kinetics as the corresponding wild-type (WT) virus (Fig. 3a). Upon infection of NIH-3T3 fibroblasts with the respective viruses at an m.o.i. of 5, we quantified IE3, IE1 and β-tubulin (control) protein expression at 24, 48 and 72 hpi by Western blot (Fig. 3b and c). However, no differences in IE3 expression were observed.
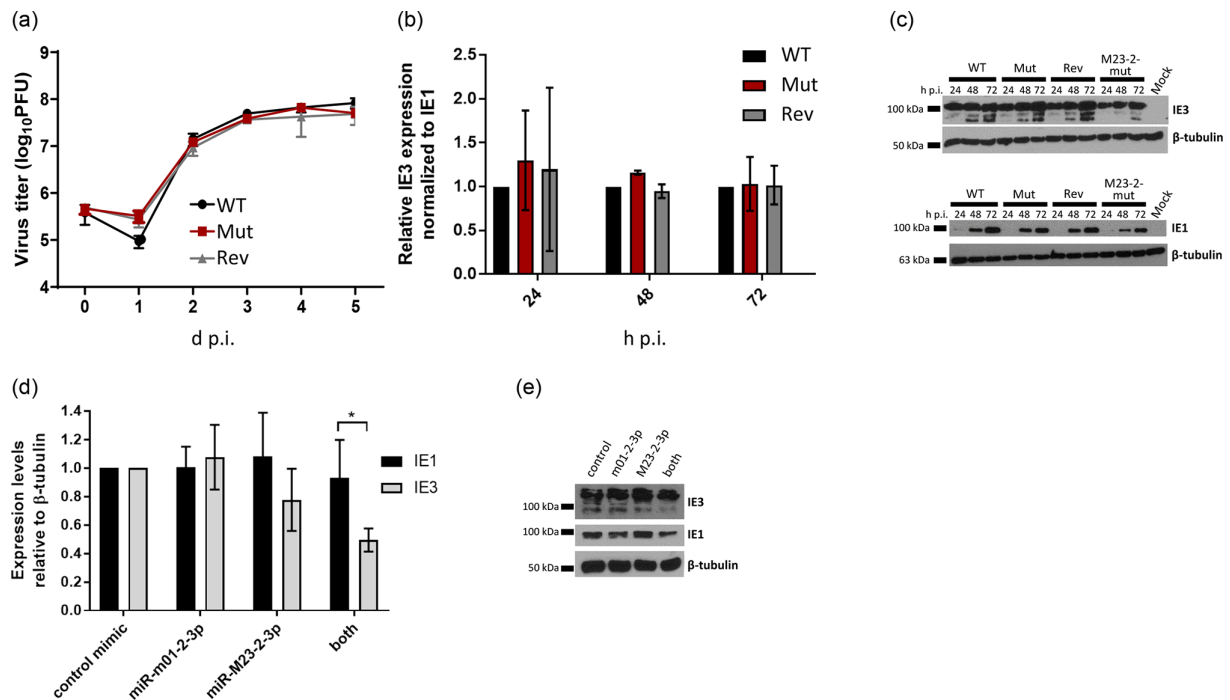
Fig. 3. (a) *In vitro* multi-step growth curves from primary BALB/c MEF for wild-type (WT), *ie3*-mutant (Mut; Clone 2–2) and the corresponding revertant (Rev; Clone 2-2-1) virus are shown. Cells were infected at an m.o.i. of 0.1. At the indicated days post-infection (dpi), the triplicates of the cell-free culture supernatants were collected and stored at −80 °C. The amount of extracellular infectious virus present in the culture supernatant was subsequently determined by a standard plaque-forming assay. Non-parametric Kruskal–Wallis one-way ANOVA was used for statistical analysis. No statistical differences in titres between the respective viruses were observed at any of the specific time points. (b) To assess the effect of endogenous viral miRNA expression on IE3 expression, NIH-3T3 cells were seeded in 24-well plates at 6.4×10^4 cells per well. Then, 24 h later cells were infected with wild-type (WT) MCMV, its *ie3* miRNA binding site mutant (Mut, Clone 2-2) and the corresponding revertant (Rev, Clone 2-2-1) at an m.o.i. of 5. At 24, 48 and 72 hpi cells were harvested and subjected to Western blot analysis for IE3, IE1 and *β*-tubulin (control) expression. Combined data of three independent experiments are shown. (c) A representative experiment, which included infection with a mutant virus lacking miR-M23-2 and miR-m21-1 [19]. (d) To assess the effect of viral miR-M23-2 and miR-m01-2 on IE3 protein expression when the miRNAs are already present in the cells prior to infection, NIH-3T3 cells were seeded in 24-well plates at 6.4×10^4 cells per well. Then, 24 h later, cells were transfected with the respective miRNA mimics [the two viral miRNAs either individually (50 pmol) or combined (25+25 pmol), or a control miRNA] and 100 ng of pDsRed plasmid for transfection control in 50 µl Opti-MEM using 2 µl of lipofectamin according to the manufacturer's instructions. Two hours later, cells were again transfected using the same conditions. Twenty-four hours after the second transfection, cells were infected with wild-type MCMV at an m.o.i. of 1. Samples were harvested for Western blot analysis at 48 hpi probing for IE3, IE1 and *β*-tubulin expression. Combined data of four independent experiments are shown. (e) A representative experiment. Significance was calculated using a two-tailed paired Student's *t*-test. *P=0.025.

To assess the impact of viral miR-M23-2 and miR-m01-2 on IE3 protein expression when the miRNAs are already present prior to infection, we transfected NIH-3T3 fibroblasts with the two viral miRNAs either individually or combined (or a control miRNA) twice within 2 h. Then, 24 h later, we infected the cells with wild-type MCMV at an m.o.i. of 1. Expression of viral IE3 and IE1 as well as β-tubulin at 48 hpi was quantified by Western blot (Fig. 3d and e). While miR-m01-2 had no effect, and miR-M23-2 showed a trend towards reduced IE3 protein expression, combined pre-expression of the two miRNAs significantly (*P*=0.025) inhibited expression of IE3 but not IE1 gene expression.

Pre-expression of the two viral miRNAs inhibits the initiation of productive infection

To directly assess the impact of the two MCMV miRNAs on the initiation of lytic infection, we analysed the initiation of virus plaques in NIH-3T3 cells transfected with the respective viral miRNAs. As a positive control, we utilized an siRNA targeting the *ie3* 3′-UTR in between the two MCMV miRNA binding sites (untouched by the introduced point mutations). As expected, dual luciferase reporter assays confirmed strong repression of both the wild-type (p/IE3) and the double miRNA binding site mutant reporter (p/IE3-mut) by the IE3 siRNA (Fig. 4a). To directly monitor both early and late viral gene expression, we utilized a dual-colour reporter virus, which expresses eGFP with early kinetics in the m152 locus (thereby replacing the m152 coding sequence) and mCherry with late kinetics driven by an EMCV internal ribosome entry sites (IRES) within the m48.2 (small capsid protein) 3′-UTR. On the genetic background of this dual-colour reporter virus, we jointly mutated both MCMV miRNA binding sites to match the p/IE3-mut reporter and generated the corresponding revertant virus by restoring the *ie3* 3′-UTR
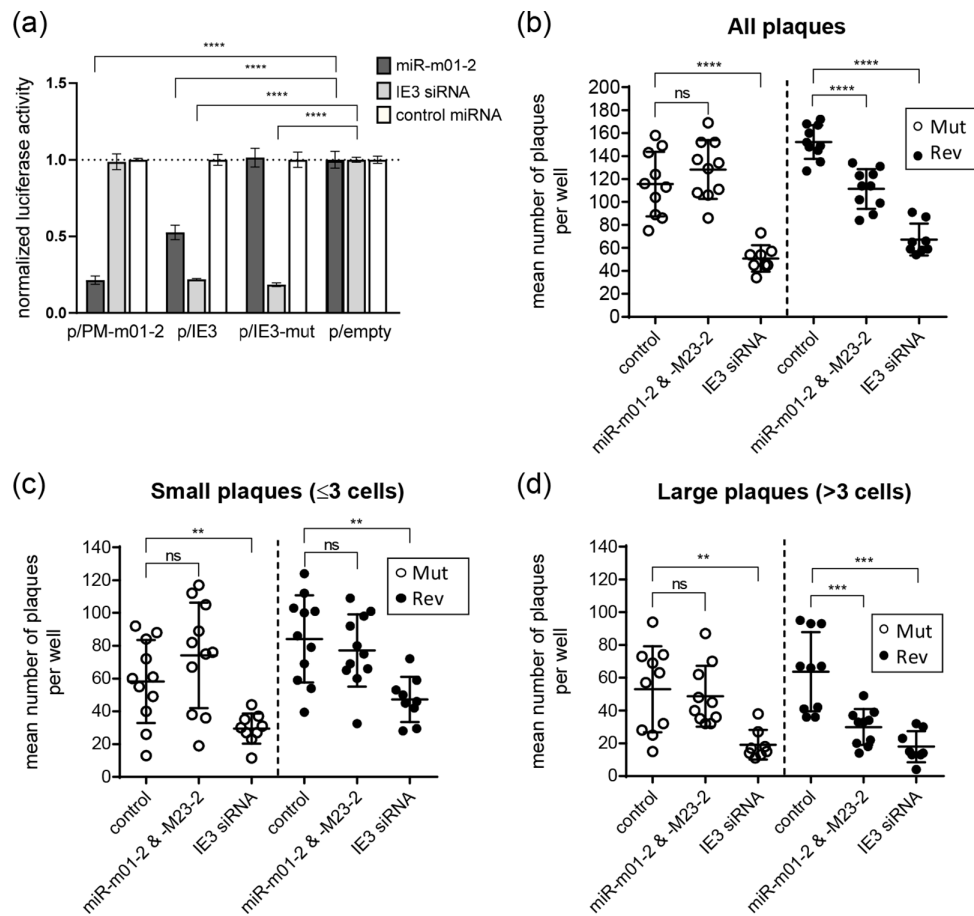
Fig. 4. Pre-expression of the two MCMV miRNAs interferes with the initiation of productive infection. (a) Dual luciferase assays confirm repression of both wild-type and mutant *ie3* 3′-UTR reporters by an siRNA targeting the region between the two MCMV miRNA binding sites. HEK293T cells were co-transfected with the indicated dual luciferase reporters and either miR-m01-2, a negative control miRNA or an siRNA targeting the *ie3* 3′-UTR in between the two MCMV miRNA binding sites. Normalized firefly luciferase activities are shown. p/PM-m01−2=perfect match reporter for viral miR-m01-2-3p. p/empty=negative control reporter. Combined data (mean±SEM) of two independent experiments are shown. ****$P<0.0001$. (b–d) Plaque repression assays demonstrate inhibition of productive infection upon pre-expression of both miR-M23-2 and miR-m01-2. NIH-3T3 fibroblasts were reverse transfected with 50 nM of both miR-m01-2 and miR-M23-2 mimics, the siRNA targeting *ie3* or a control fluorescent miRNA mimic (control). Then, 24 h post-transfection, cells were infected at low multiplicity of infection (aiming for ~100 plaques per well of a 48-well plate) with either the *ie3* 3′-UTR mutant virus (both MCMV miRNA binding sites mutated) or its revertant. Fluorescent plaques were counted 3 days later. Based on the number of red fluorescent cells (late-stage infection), plaques were grouped into small (three or fewer infected cells) and large plaques (more than three infected cells). Combined data of two independent experiments performed on either 10 (eight for siRNA-transfected samples) individual wells are shown. Mean number of plaques per well ±SD is shown. **$P<0.01$; ***$P<0.001$; ****$P<0.0001$.

wild-type sequence. We subsequently reversely transfected (i) both miR-m01-2 and miR-M23-2, (ii) the siRNA to *ie3* (positive control), or (iii) a negative control miRNA into NIH-3T3 cells. Then, 24 h later, we infected the cells at very low m.o.i. with either the mutant virus or its revertant aiming for ~100 plaques per well of a 48-well plate. While pre-expression of both miR-M23-2 and miR-m01-2 had no effect on the number of arising plaques of the mutant virus, the number of plaques observed for the revertant virus was significantly reduced (Fig. 4b; $P<0.0001$). In contrast, the siRNA against the *ie3* 3′-UTR repressed both the mutant and revertant virus, consistent with strong repressive effects of this siRNA on both the wild-type and mutant *ie3* 3′-UTR dual luciferase reporter constructs (Fig. 4a). Interestingly, miRNA pre-expression most strongly affected the number of large plaques comprising more than three infected cells (>2-fold; Fig. 4c), while no effect was observed for small plaques with about three infected cells (Fig. 4d). This indicates that miRNA pre-expression predominantly suppresses but not eliminates the invading viral genomes thereby delaying the onset of infection and thus plaque size.

Repression of *ie3* does not affect acute infection *in vivo*

To analyse the role of the two *ie3* binding sites on the viral fitness in mice, we not only utilized the wild-type virus (m129 repaired), its *ie3* dual miRNA binding site mutant (Clone 2-2) and revertant virus (Clone 2-2-1), but also reconstituted a second independent
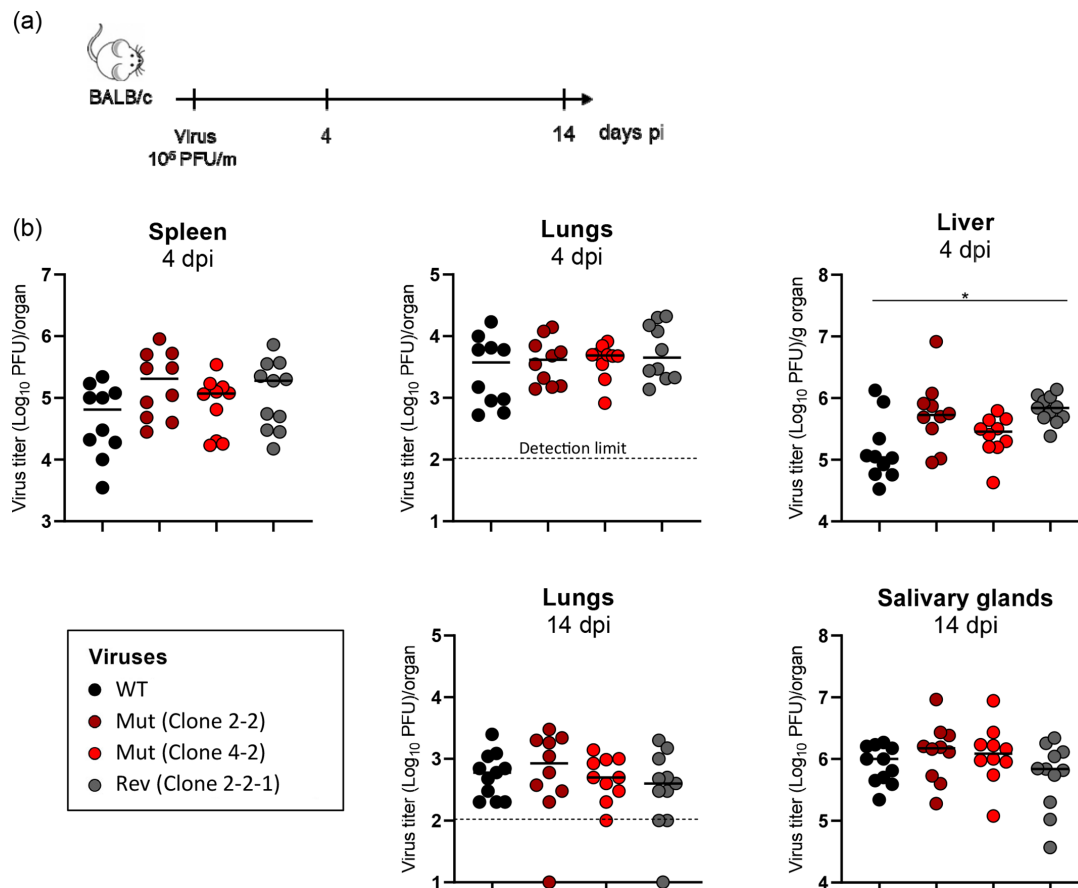
Fig. 5. Differential expression of *ie3* does not affect control of acute and subacute MCMV infection. (a) BALB/c mice were infected with 10^5 p.f.u. of WT, the two *ie3* mutants (Clone 2-2 and Clone 4–2) or the revertant of Clone 2-2 (Clone 2-2-1). (b) Viral titres in the indicated organs were determined by plaque assay at 4 dpi (intravenous infection, i.v.) and 14 dpi (intraperioneal infection, i.p.). Graphs show two merged experiments with five mice per group. Each circle represents an individual animal and bold lines represent medians. The dashed line represents a line of plaque detection. Unpaired one-way ANOVA (Kruskall–Wallis H-test) was used for statistical analysis. Asterisks denote significant values: *$P \leq 0.05$.

mutant clone (Clone 4-2). To assess the relevance of *ie3* regulation by the two MCMV miRNAs for productive infection *in vivo*, we infected BALB/c mice with 1×10^5 p.f.u. of wild-type MCMV, the two mutant clones as well as the revertant virus. All viruses replicated to similar titres in lungs, liver and spleen by 4 dpi as well as in lungs and salivary glands by 14 dpi (Fig. 5). Identical results were obtained when infecting BALB/c mice with low dose (2×10^4 p.f.u. per mouse) of either mutant (Clone 2-2) or revertant virus (Clone 2-2-1) for 4 days (lung, spleen and liver) or 14 days (lung and salivary glands) (Fig. S5). Apparently, regulation of *ie3* by the respective viral miRNAs does not play a major role in both acute and subacute infection *in vivo*.

Repression of *ie3* does not affect CD8$^+$ T-cell responses

Regulation of *ie3* expression by viral miRNAs may play a role in the establishment of viral latency or reactivation thereof. Even in immunocompetent mice, subclinical virus reactivation over time results in the continuous expansion of virus-specific T cells, a process termed memory inflation [31]. To assess the role of miRNA-mediated regulation of *ie3* over time, we analysed T-cell responses against both conventional and inflated viral CD8$^+$ T-cell epitopes in both BALB/c and C57BL/6 mice infected with 10^5 p.f.u. of either mutant (Clone 2-2) or its revertant virus (Clone 2-2-1) over up to 1 year. Virus-specific CD8$^+$ T cells for different viral epitopes were determined by intracellular cytokine staining (IFNγ) and flow cytometry. In BALB/c mice, virus-specific CD8$^+$ T cells for an epitope of either m164 or IE1 (pp89) were measured in three mice at 9, 14, 30, 120 and 365 dpi. Of note, both mutant and revertant virus induced identical numbers of virus-specific CD8$^+$ T cells (Fig. 6a). In C57BL/6 mice, virus-specific CD8$^+$ T cells against epitopes from M38, M45, m139 and *ie3* were measured at 4 and 12 months post-infection. As observed for BALB/c mice, mutation of the *ie3* miRNA binding sites had no significant effect on the number of virus-specific CD8$^+$ T cells for any of the analysed epitopes including *ie3* (Fig. 6b). To answer the question of whether differential regulation of *ie3* expression affects differentiation and heterogeneity of virus-specific memory CD8$^+$ T cells, we infected BALB/c mice with 10^5 p.f.u. of either *ie3* mutant (Clone 2-2) or revertant MCMV (Clone 2-2-1) and analysed the phenotype of CD8$^+$ T cells at day 550 post-infection
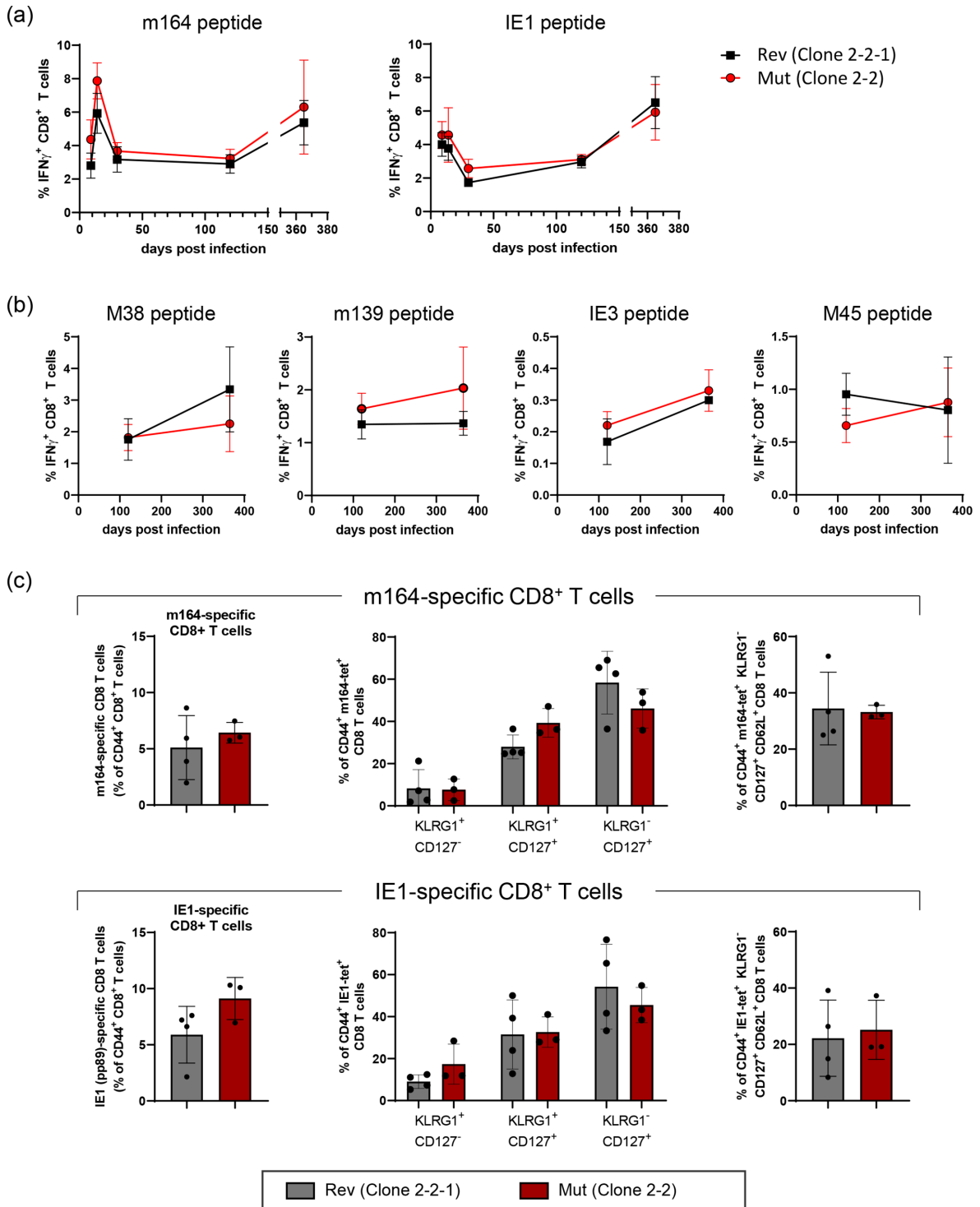
Fig. 6. miRNA-mediated regulation of *ie3* has no significant impact on the antiviral CD8⁺ T-cell response. BALB/c (a, c) and C57BL/6 (b) mice were footpad inoculated with 10^5 p.f.u. per mouse of the *ie3* mutant (Clone 2-2) virus or its revertant virus (Clone 2-2-1). (a–b) At the indicated days post-infection (dpi), splenocytes were isolated and incubated with virus-specific peptides in the presence of Brefeldin for 5 h. Production of IFNγ was measured by flow cytometry. Two-way ANOVA was used for statistical analysis. (c) At 550 dpi, splenocytes were stained with MCMV m164- and IE1 (pp89)-specific tetramers together with markers for memory CD8⁺ T-cell differentiation. Graphs on the left show percentages of virus-specific CD8⁺ T cells. Middle graphs represent the percentage of virus-specific CD44⁺KLRG1⁺CD127⁻, CD44⁺KLRG1⁺CD127⁺ and CD44⁺KLRG1⁻CD127⁺ populations. Right graphs show virus-specific central memory CD8⁺ T cells (CD44⁺KLRG1⁻CD127⁺CD62L⁺). Data were analysed using either an unpaired Student's *t*-test or one-way ANOVA. Graphs show mean with SD as error bars.

(Fig. 6c and Fig. S6). No significant differences in the frequency of virus-specific memory CD8$^+$ T-cell subsets between mutant and revertant virus were observed. Thus, repression of *ie3* by the two viral miRNAs does not influence the frequency or phenotype of MCMV-specific memory CD8$^+$ T cells.

We conclude that regulation of *ie3* by viral miR-M23-2 and miR-m01-2 has little impact on the establishment of latency and subclinical virus reactivation in immunocompetent, healthy laboratory mice when mice are housed in an infection-free environment.

DISCUSSION

We employed PAR-iCLIP to identify targets of the MCMV miRNAs during productive infection of fibroblasts and epithelial cells. While we observed a highly significant enrichment of seed matches for cellular and viral miRNAs in the obtained cellular PAR-iCLIP reads, the signal-to-noise ratio within the cellular transcriptome was not sufficient to identify the hundreds to thousands of miRNA target sites previously reported for other viruses [32–34]. In contrast, we identified a PAR-iCLIP peak in the *ie3* transcript as the most striking PAR-iCLIP cluster within the viral genome. The increased signal-to-noise ratio for the viral transcriptome probably stems from higher 4sU incorporation rates within the viral mRNAs, which are only transcribed in the presence of 4sU.

We show that the PAR-iCLIP cluster in the *ie3* 3′-UTR reflects the interaction of the *ie3* transcript with two of the most abundant MCMV miRNAs, namely miR-M23-2-3p and miR-m01-2-3p, which cooperate in the regulation of *ie3* expression. IE3 is the MCMV homologue of the HCMV IE86 gene, the major viral transcription factor that is essential for viral early and late gene expression. As previously reported for miR-UL112-1 in HCMV, pre-expression of the two MCMV miRNAs inhibited plaque formation and thus productive virus replication in fibroblasts. This was fully reversed upon mutation of miRNA seed matches (exchange of 3 nt in each of the two miRNA binding sites) within the *ie3* 3′-UTR. Nevertheless, disruption of miRNA-mediated suppression of *ie3* had no measurable effect on productive virus replication during both acute and subacute infection in mice.

We hypothesized that suppression of *ie3* expression via the two viral miRNAs might affect the establishment of viral latency or reactivation in the long term. However, viral loads in various organs in latency are difficult to quantify due to the low levels of viral genomes in cells. Although transcripts from the immediate early region can be detectable in some cases, the large part of a genome is transcriptionally silent in latently infected mice [35]. Moreover, the induction of MCMV productive reactivation usually results in viral titres that could mask small differences in the quantity of the viral genome, which could be otherwise attributed to miRNA-mediated regulation of the *ie3* gene region. At the same time, after resolving acute infection and establishment of latency, a pool of MCMV-specific CD8$^+$ T cells gradually increases as a result of subclinical virus reactivation in a process termed memory inflation [31]. We exploited this phenomenon to test whether miRNA-mediated *ie3* regulation could affect CD8$^+$ T-cell memory profiles functionally and phenotypically. However, neither type of experiment yielded significant differences in CD8$^+$ T-cell profiles in mice infected with WT/revertant virus and *ie3* mutants for up to 1 year. We concluded that miRNA-mediated regulation of *ie3* does not affect the establishment of viral latency and reactivation in healthy laboratory mice housed under pathogen-free conditions, at least not in a way that could permanently affect CD8$^+$ T-cell memory heterogeneity and functionality. The observed absence of differences in CD8$^+$ T-cell phenotype could also be explained by the ability of MCMV to skew CD8$^+$ T-cell recognition early upon infection by multiple different mechanisms to ensure life-long persistence in the host.

Repression of viral immediate early gene expression is a generalized feature of herpesvirus miRNAs, which independently arose in alpha, beta and gamma herpesviruses [10]. This suggests an important role of this type of regulation for these viruses. For HCMV, inhibition of IE72 gene expression by viral miR-UL112-1 prevented recognition and killing of HCMV-infected cells in an HCMV latency model *in vitro* [16]. This is of particular importance as up to >10% of all CD8$^+$ T cells in healthy individuals recognize the HCMV IE72 antigen [36, 37]. However, disrupting the inhibition of IE72 gene expression by miR-UL112-1 was not sufficient to trigger virus reactivation in virus co-culture analysis [16]. Interestingly, host miRNAs have also been shown to regulate herpesvirus immediate early protein expression to promote viral latency [38, 39]. Cells permissive for lytic replication of the respective viruses (HCMV and HSV-1) generally demonstrate low levels of these miRNAs. Herpesviruses thus utilize both cellular and viral miRNAs to regulate immediate early gene expression for control latency establishment, maintenance or reactivation thereof.

All cytomegaloviruses thrive in inflammatory environments such as infections with other pathogens. As miRNAs are generally long-lived it is tempting to speculate that viral miRNAs targeting the major viral immediate early proteins such as IE3 may become functionally relevant in biological settings when virus reactivations are much more frequent than in the current pathogen-free laboratory settings. Future work in more natural settings with frequent infections by other pathogens will probably be required to elucidate the functional role of viral miRNA-mediated regulation of key viral immediate early proteins.

Funding information

Acknowledgements

Author contributions

Conflicts of interest

The authors declare no conflicts of interest.

Ethical statement

All the protocols used for breeding of mice and different kinds of treatments were approved by the Ethical Committee of the Faculty of Medicine University of Rijeka and were performed in accordance with Croatian Law for the Protection of Laboratory Animals, which has been harmonized with the existing EU legislation (EC Directive 86/609/EEC).

References

1. Mocarski ES, Shenk T. Cytomegalovirus. In: *Fields Virology*. Lippincott Williams & Wilkins, 2013.

2. Hook L, Hancock M, Landais I, Grabski R, Britt W, et al. Cytomegalovirus microRNAs. *Curr Opin Virol* 2014;7:40–46.

3. Poole E, Sinclair J. Sleepless latency of human cytomegalovirus. *Med Microbiol Immunol* 2015;204:421–429.

4. Zhang L, Yu J, Liu Z. MicroRNAs expressed by human cytomegalovirus. *Virol J* 2020;17:34.

5. Diggins NL, Skalsky RL, Hancock MH. Regulation of latency and reactivation by human cytomegalovirus miRNAs. *Pathogens* 2021;10:1–15.

6. Hook L, Hancock M, Landais I, Grabski R, Britt W, et al. Cytomegalovirus microRNAs. Curr Opin Virol 2014;7:40–46.

7. Goldberger T, Mandelboim O. The use of microRNA by human viruses: lessons from NK cells and HCMV infection. *Semin Immunopathol* 2014;36:659–674.

8. Diggins NL, Hancock MH. HCMV miRNA Targets Reveal Important Cellular Pathways for Viral Replication, Latency, and Reactivation. *Noncoding RNA* 2018;4:E29.

9. Stern-Ginossar N, Elefant N, Zimmermann A, Wolf DG, Saleh N, et al. Host immune system gene targeting by a viral miRNA. *Science* 2007;317:376–381.

10. Murphy E, Vaníček J, Robins H, Shenk T, Levine AJ. Suppression of immediate-early viral gene expression by herpesvirus-coded microRNAs: implications for latency. *Proc Natl Acad Sci* 2008;105:5453–5458.

11. Grey F, Meyers H, White EA, Spector DH, Nelson J. A human cytomegalovirus-encoded microRNA regulates expression of multiple viral genes involved in replication. *PLoS Pathog* 2007;3:e163.

12. Pegtel DM, Cosmopoulos K, Thorley-Lawson DA, van Eijndhoven MAJ, Hopmans ES, et al. Functional delivery of viral miRNAs via exosomes. *Proc Natl Acad Sci* 2010;107:6328–6333.

13. Bellare P, Ganem D. Regulation of KSHV lytic switch protein expression by a virus-encoded microRNA: an evolutionary adaptation that fine-tunes lytic reactivation. *Cell Host Microbe* 2009;6:570–575.

14. Jung Y-J, Choi H, Kim H, Lee SK. MicroRNA miR-BART20-5p stabilizes Epstein-Barr virus latency by directly targeting BZLF1 and BRLF1. *J Virol* 2014;88:9027–9037.

15. Umbach JL, Kramer MF, Jurak I, Karnowski HW, Coen DM, et al. MicroRNAs expressed by herpes simplex virus 1 during latent infection regulate viral mRNAs. *Nature* 2008;454:780–783.

16. Lau B, Poole E, Van Damme E, Bunkens L, Sowash M, et al. Human cytomegalovirus miR-UL112-1 promotes the down-regulation of viral immediate early-gene expression during latency to prevent T-cell recognition of latently infected cells. *J Gen Virol* 2016;97:2387–2398.

17. Dölken L, Perot J, Cognat V, Alioua A, John M, et al. Mouse cytomegalovirus microRNAs dominate the cellular small RNA profile during lytic infection and show features of posttranscriptional regulation. J Virol 2007;81:13771–13782.

18. Buck AH, Santoyo-Lopez J, Robertson KA, Kumar DS, Reczko M, et al. Discrete clusters of virus-encoded MicroRNAs are associated with complementary strands of the genome and the 7.2-kilobase stable intron in murine cytomegalovirus. *J Virol* 2007;81:13761–13770.

19. Dölken L, Krmpotic A, Kothe S, Tuddenham L, Tanguy M. Cytomegalovirus microRNAs facilitate persistent virus infection in salivary glands facilitate persistent virus infection in salivary glands. *PLoS Pathog* 2010;6:e1001150.

20. Tischer BK, Smith GA, Osterrieder N. En passant mutagenesis: a two step markerless red recombination system. *Methods Mol Biol* 2010;634:421–430.

21. Reddehase MJ, Weiland F, Münch K, Jonjic S, Lüske A, et al. Interstitial murine cytomegalovirus pneumonia after irradiation: characterization of cells that limit viral replication during established infection of the lungs. *J Virol* 1985;55:264–273.

22. Marcinowski L, Tanguy M, Krmpotic A, Rädle B, Lisnić VJ, et al. Degradation of cellular mir-27 by a novel, highly abundant viral transcript is important for efficient virus replication in vivo. *PLoS Pathog* 2012;8:e1002510.

23. Marcinowski L, Lidschreiber M, Windhager L, Rieder M, Bosse JB, et al. Real-time transcriptional profiling of cellular and viral gene expression during lytic cytomegalovirus infection. *PLoS Pathog* 2012;8:e1002908.

24. Brune W, Hengel H, Koszinowski UH. A mouse model for cytomegalovirus infection. *Curr Protoc Immunol* 2001;Chapter 19:Unit .

25. Konig J, Zarnack K, Rot G, Curk T, Kayikci M, et al. iCLIP--transcriptome-wide mapping of protein-RNA interactions with individual nucleotide resolution. *J Vis Exp* 2011::2638.

26. Davis MPA, van Dongen S, Abreu-Goodger C, Bartonicek N, Enright AJ. Kraken: a set of tools for quality control and analysis of high-throughput sequence data. *Methods* 2013;63:41–49.

27. Langmead B, Trapnell C, Pop M, Salzberg SL. Ultrafast and memory-efficient alignment of short DNA sequences to the human genome. *Genome Biol* 2009;10:R25.

28. Jürges C, Dölken L, Erhard F. Dissecting newly transcribed and old RNA using GRAND-SLAM. *Bioinformatics* 2018;34:i218–i226.

29. Hafner M, Landthaler M, Burger L, Khorshid M, Hausser J, et al. (n.d.) PAR-CliP - a method to identify transcriptome-wide the binding sites of RNA binding proteins. *JoVE*

30. **Rehmsmeier M, Steffen P, Hochsmann M, Giegerich R**. Fast and effective prediction of microRNA/target duplexes. *RNA* 2004;10:1507–1517.

31. **Karrer U, Sierro S, Wagner M, Oxenius A, Hengel H**, *et al.* Memory inflation: continuous accumulation of antiviral CD8+ T cells over time. *J Immunol* 2003;170:2022–2029.

32. **Skalsky RL, Corcoran DL, Gottwein E, Frank CL, Kang D**, *et al.* The viral and cellular microRNA targetome in lymphoblastoid cell lines. *PLoS Pathog* 2012;8:e1002484.

33. **Gottwein E, Corcoran DL, Mukherjee N, Skalsky RL, Hafner M**, *et al.* Viral microRNA targetome of KSHV-infected primary effusion lymphoma cell lines. *Cell Host Microbe* 2011;10:515–526.

34. **Gay LA, Sethuraman S, Thomas M, Turner PC, Renne R**. Modified cross-linking, ligation, and sequencing of hybrids (qCLASH) Identifies Kaposi's Sarcoma-associated herpesvirus MicroRNA targets in endothelial cells. *J Virol* 2018;92:e02138-17.

35. **Reddehase MJ, Simon CO, Seckert CK, Lemmermann N, Grzimek NKA**. Murine model of cytomegalovirus latency and reactivation. *Curr Top Microbiol Immunol* 2008;325:315–331.

36. **Kern F, Surel IP, Brock C, Freistedt B, Radtke H**, *et al.* T-cell epitope mapping by flow cytometry. *Nat Med* 1998;4:975–978.

37. **Gillespie GM, Wills MR, Appay V, O'Callaghan C, Murphy M**, *et al.* Functional heterogeneity and high frequencies of cytomegalovirus-specific CD8(+) T lymphocytes in healthy seropositive donors. *J Virol* 2000;74:8140–8150.

38. **O'Connor CM, Vanicek J, Murphy EA**. Host microRNA regulation of human cytomegalovirus immediate early protein translation promotes viral latency. *J Virol* 2014;88:5524–5532.

39. **Pan D, Flores O, Umbach JL, Pesola JM, Bentley P**, *et al.* A neuron-specific host microRNA targets herpes simplex virus-1 ICP0 expression and promotes latency. *Cell Host Microbe* 2014;15:446–456.